ACS APPLIED MATERIALS & INTERFACES

Research Article

www.acsami.org

Liquid Crystal Elastomer Microspheres as Three-Dimensional Cell Scaffolds Supporting the Attachment and Proliferation of Myoblasts

Tanmay Bera,[‡,§] Ernest J. Freeman,[§] Jennifer A. McDonough,[§] Robert J. Clements,[§] Asaad Aladlaan,[∥] Donald W. Miller,[#] Christopher Malcuit,*[,§] Torsten Hegmann,[†,‡,⊥,#] and Elda Hegmann*[,‡,§,⊥]

[†]Chemical Physics Interdisciplinary Program, [‡]Liquid Crystal Institute, [§]Department of Biological Sciences, [∥]School of Biomedical Sciences, and [⊥]Department of Chemistry and Biochemistry, Kent State University, Kent, Ohio 44242-001, United States

[#]Department of Pharmacology and Therapeutics, University of Manitoba, Winnipeg, MB R3E 0T6, Canada

Supporting Information

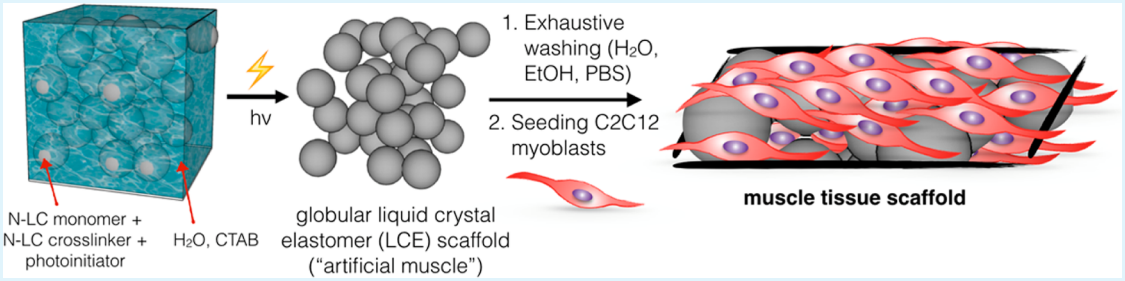

ABSTRACT: We report that liquid crystal elastomers (LCEs), often portrayed as artificial muscles, serve as scaffolds for skeletal muscle cell. A simultaneous microemulsion photopolymerization and cross-linking results in nematic LCE microspheres 10−30 μm in diameter that when conjoined form a LCE construct that serves as the first proof-of-concept for responsive LCE muscle cell scaffolds. Confocal microscopy experiments clearly established that LCEs with a globular, porous morphology permit both attachment and proliferation of C2C12 myoblasts, while the nonporous elastomer morphology, prepared in the absence of a microemulsion, does not. In addition, cytotoxicity and proliferation assays confirm that the liquid crystal elastomer materials are biocompatible promoting cellular proliferation without any inherent cytotoxicity.

KEYWORDS: *liquid crystal elastomer, artificial muscle, 3D cell scaffold, microspheres, myoblasts, cell proliferation*

INTRODUCTION

While many biologic and synthetic materials have been tested for skeletal muscle tissue engineering, the field has reached a consensus about critical criteria to support regeneration of this tissue. Such a material should promote adhesion, proliferation, and differentiation of skeletal myoblasts while approximating both the mechanical properties of skeletal muscle and allowing guidance as well as alignment of endogenous (perhaps also exogenous) muscle cell growth.[1]

Liquid crystal elastomers (LCEs) are unique synthetic, cross-linked polymers featuring orientational ordering and attractive mechanical and optical properties.[2,3] Of the numerous potential applications for LCEs, sensors and actuators have been the most promising.[4−22] This is due to their ability to undergo significant shape change in response to external stimuli,[15,23−35] where their anisotropic response sets them apart from conventional elastomer materials. Their soft and malleable nature allows them to conform to different shapes and surfaces.[36] Some reports highlight that the contractile and expansion properties of these materials are associated with forces on the order of ∼210 kPa, leading to the concept that LCEs can be used as artificial muscles or biologically relevant actuators.[8,9,37−46] Terentjev et al., for example, showed that anisotropic LCE microparticles (anisotropic colloidal micro-muscles) could be thermally triggered for reversible shape change (potentially up to 500% strain change for main-chain LCEs), and that the level of stress holding made them mechanically similar to natural muscle.[9] De Gennes first proposed the idea of nematic gels and LCEs as artificial muscles.[47,48] Surprisingly no study on the biological use of LCEs as cell scaffolds for muscle cells has been reported to date. Most likely, the key reasons for this is the hydrophobic nature of most LCEs composed of common mesogenic building blocks and the lack of suitable LCE morphologies allowing for cell attachment. The similarity of the mechanic response of LCEs to that of natural muscle tissue, the responsiveness to external stimuli, and the dynamic self-stiffening should provide an active scaffold ideal for muscle cell attachment and proliferation ultimately leading to the generation of many types of engineered tissue.[37] Recent research has shown that the physical parameters of cell substrates are essential for controlling biological responses of

Received: May 15, 2015
Accepted: June 15, 2015
Published: June 15, 2015

DOI: 10.1021/acsami.5b04208
ACS Appl. Mater. Interfaces 2015, 7, 14528−14535

cells. These parameters include matching the mechanical properties, the size and shape of nano- or microparticles, the surface microstructure, the texture, and the porosity.[49] Normal tissue cells including muscle cells, neurons, or other tissue and stem cells[50] sense the elasticity of their environment or substrate as they anchor to it.[51] The anisotropic nature of LCEs would provide a suitable substrate to support three-dimensional (3D) cell growth.

We have shown earlier that smectic LCEs with internal porosity promote cell adhesion and permeation into an LCE scaffold.[52] Using a microemulsion photopolymerization method, we provide the first proof-of-concept study on the utilization of LCEs as 3D scaffolds for muscle cells.[9,53−62] The resulting LCEs have a globular morphology characterized by an overall rough surface and pores suited for 3D cell scaffolds. The LCEs feature a more porous, globular morphology, with internal pores that allow for complete fluid penetration and exchange. In comparison, LCEs made in the absence of a microemulsion will proof to be dense, thus lacking the desired porosity and overall surface roughness for cell adhesion, and proliferation.

MATERIALS AND METHODS

Materials. The monomer (M), 4-(heptyloxy)phenyl 4-((6-(acryloyloxy)hexyl)oxy)benzoate and the cross-linker (CL) 1,4-bis-[4-(6-acryloyloxyhexyloxy)benzoyloxy]-2-methylbenzene were purchased from Synthon Chemicals GmbH (Germany). The photoinitiator (PI) 2,2-dimethyoxy-2-phenylacetophenone and the surfactant hexadecyltrimethylammonium bromide (CTAB) were purchased from Sigma-Aldrich. Toluene (EMD Millipore grade, purified by a PureSolv solvent purification system, Innovative Technology, Inc.) and deionized (DI) water (Millipore, resistivity 18.1 MΩ) were used as solvents.

Materials Characterization. Polarized optical microscopy was done using an Olympus BX53 (bright field and crossed polarizers). Confocal microscopy was carried out using an Olympus FV1000; ImageJ[63] was used for image analysis/processing. Scanning electron microscopy was performed using a Hitachi S-2600N. Samples were sputter-coated with Pd−Au. For Fourier transform infrared (FT-IR) spectroscopy, the elastomers were mixed with anhydrous KBr (VWR), then ground, and pressed into pellets. Their IR-absorption spectrum was recorded using a Magna Nicolet 500 FT-IR spectrometer. Phase transitions temperatures and enthalpies of the elastomers were obtained by differential scanning calorimetry using a PerkinElmer Pyris 1 at a scan rate of 5 °C/min from −60 to 250 °C under a N_2 atmosphere. Thermal degradation was studied using a Hi Res TGA-2950 (TA Instruments) at a ramp rate of 10 °C/min.

Elastomer Synthesis. The method used for the synthesis of the LCE microsphere scaffolds followed, with some modifications, the standard photopolymerization reaction of acrylate-based, nematic phenylbenzoate LC elastomers reported in the literature.[64,65] In short, the conventional synthesis (without the emulsion phase) of the LC elastomer starts with accurately weighing the monomer (86 wt %), cross-linker (10 wt %), and photoinitiator (4 wt %) and transferring them to a clean glass vial. They were then dissolved in anhydrous toluene followed by UV induced photopolymerization reaction, which yields the LCEs. The photopolymerization was initiated with 365 nm UV irradiation for 15 min followed by tightly sealing the vial and heating it to 50 °C. The heating was continued for 12 h in a temperature controlled sand bath, which completes the polymerization reaction. Thereafter, the excess toluene/water azeotrope was evaporated at reduced pressure and the elastomer samples were recovered by breaking the vial. They were then exhaustively washed with water and ethanol to remove any unreacted monomers and surfactant. Finally, the elastomer samples were air-dried and carefully stored for further analysis.

For the microemulsion photopolymerization, the basic synthesis procedure remained the same with slight modifications. The monomer, cross-linker, and photoinitiator were first dissolved in anhydrous toluene to obtain a homogeneous solution. The toluene solution was then added to water containing 10 vol % of 10 mM aqueous CTAB. The volumes of the toluene and water were adjusted depending on the desired toluene/water proportion. For example, for the 50:50 toluene/water ratio, 250 μL of toluene was added to a glass vial containing 200 μL of DI water and 50 μL of 10 mM aqueous CTAB. The mixture was then vigorously agitated to form a milky-white toluene/water emulsion. The stable emulsion was then irradiated with 365 nm UV light to initiate the polymerization reaction. The washing and recovery of the elastomer samples remained the same ensuring that all unreacted monomers, the cross-linker, and the surfactant were completely removed.

Cell Cultures. LCE samples were seeded with murine C2C12 myoblast cells (ATCC) and cultured using standard sterile techniques. Growth medium for C2C12 contained 90% Dulbecco's modified Eagle's medium (DMEM), supplemented with 10% fetal bovine serum (FBS) and 1% penicillin/streptomycin. Prior to cell seeding, LCEs were washed with 70% ethanol, rinsed twice with phosphate buffered saline (PBS), air-dried under sterile conditions, and UV-irradiated for 30 min. They were then treated with 1 wt % poly-D-lysine solution for 2 h, rinsed with PBS, and placed carefully in 12-well cell culture plates. Approximately 5×10^4 C2C12 cells (passage 8) suspended in growth media were seeded onto each of the LCE samples. The LCEs along with the cells were incubated at 37 °C with 5% CO_2 for about 6 h to promote cell adhesion, followed by addition of growth media. Media was changed every 2 days for the first 6 days. After 7 days, cells were fixed with 4% paraformaldehyde and stained with DAPI (Life Technologies) to identify cell nuclei, and rhodamine to visualize the LCE scaffold. For 3D imaging, several images were sequentially taken and stacked into a 3D composite image using ImageJ.[63]

Cell Proliferation and Cytotoxicity Assays. Viability and proliferation of C2C12 skeletal myoblasts as well as any inherent cytoxicity of the conjugated LCE scaffolding were assessed in a complementary fashion using the PrestoBlue cell viability reagent, the CyQuant cell proliferation assay (both Life Technologies), and the CytoTox-Fluor cytotoxicity assay (Promega) according to protocols recommended by the manufacturers. For the CyQuant cell proliferation assay, the elastomer was cut into equivalent size pieces ($3 \times 3 \times 1$ mm^3) and sterilized by a 20 min incubation in 70% ethanol with three rinses of sterile Milli-Q water (EMD Millipore). The elastomer was then exposed to UV light for 15 min, and then incubated in 0.01% poly-L-lysine (Sigma P4707) for 20 min at 37 °C. Pieces of elastomer were seeded with 10,000 C2C12 skeletal myoblasts in 0.05 mL of culture medium (DMEM [Corning] + 10% FBS [Hyclone] and antibiotics [penicillin/streptomycin, Amresco]) for 2 h at 37 °C in a 5% CO_2 humidified incubator. After 2 h, elastomers with seeded myoblasts were aseptically transferred to 24-well culture plates with a 2% agarose substrate to prevent cell adhesion to the Petri dish culture surface. Elastomer/myoblast constructs were cultured for 8 days, and individual samples were removed at three time points (day 3, 5, and 8) and immediately frozen in 1.5 mL microcentrifuge tubes. At the completion of the culture period, frozen elastomer/myoblast constructs were thawed and cellular content was assessed using the CyQuant reagent according to the manufacturers recommended instructions, and fluorescence intensity was measured with excitation at 480 nm with emission at 520 nm using a Molecular Devices M4 SpectroMax multimode microplate reader. A standard curve of known C2C12 cell numbers (Supporting Information) was used to calculate the relative cell number from the mean fluorescence intensity (CyQuant $480_{Ex}/520_{Em}$). For the PrestoBlue cell viability and the CytoTox-Fluor cytotoxicity assay, C2C12 skeletal myoblasts (at 5000 cells/cm^2) were seeded into custom, nonadherent, 24-well cell culture wells containing a layer of 2% agarose (in DMEM basal medium) on the bottom, with a $3 \times 3 \times 1$ mm^3 elastomer scaffold (5.0 mg) affixed to the agarose with a 0.2 mm minutien pin (Fine Science Tools). Cultures were maintained in growth medium consisting of DMEM (Corning) with 10% FBS (Hyclone), Glutamax (Life Technologies)

DOI: 10.1021/acsami.5b04208
ACS Appl. Mater. Interfaces 2015, 7, 14528−14535

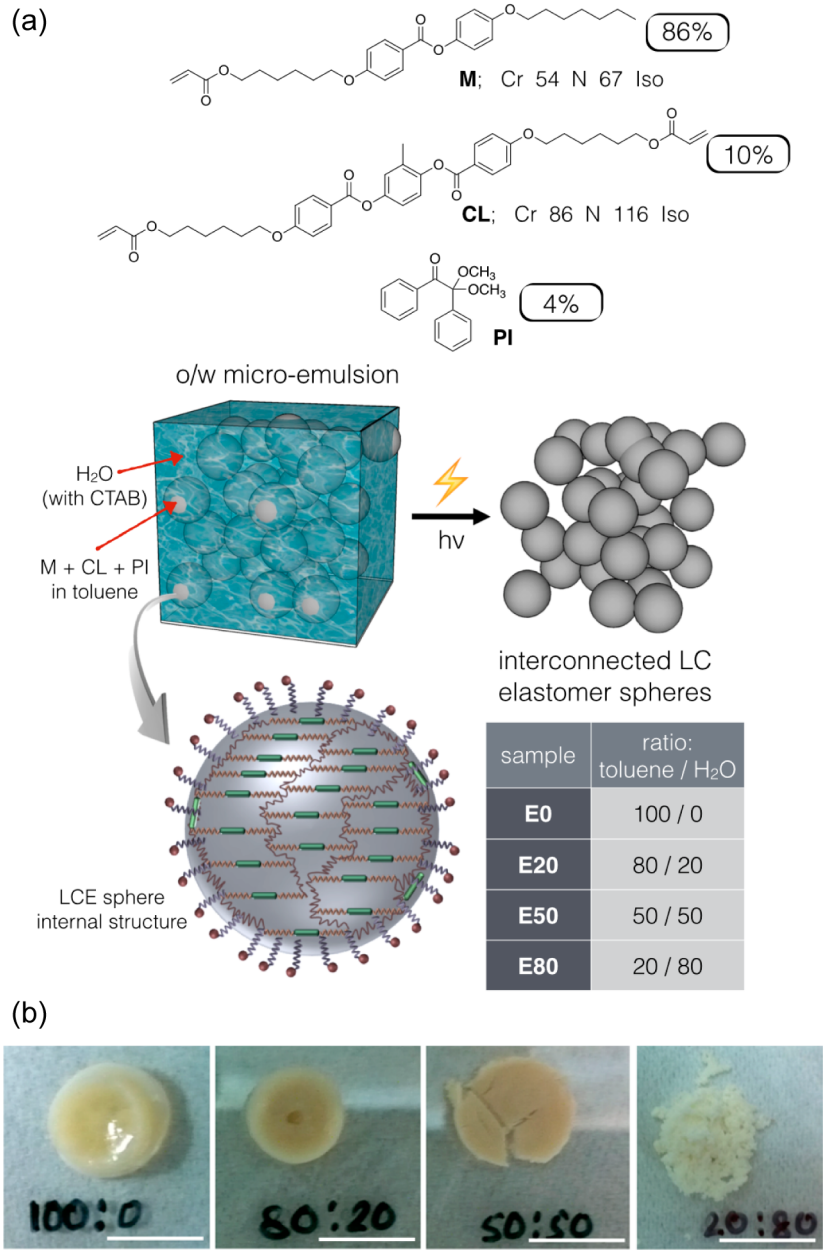

Figure 1. (a) Chemical structure, thermal behavior, and ratio of monomer (M), cross-linker (CL), and photoinitiator (PI; 2,2-dimethoxy-2-phenylacetophenone) used for the synthesis of the nematic LCE cell scaffolds. The cartoon depicts the synthesis (microemulsion photopolymerization) and the internal structure of the resulting fused LCE spheres. (b) Photographs of the four thoroughly dried LCE samples (E0, E20, E50, and E80, left-to-right). The appearance and integrity of the samples when wet (i.e., kept in culture media) is much less brittle than that after drying in a vacuum oven as shown here (i.e., fully dried for the purpose of taking the sample photographs; scale bar: 1 cm).

and penicillin/streptomycin (Amresco) for 7 days. As a control for the cytotoxicity assay, cells were also cultured in nonadherent wells without elastomer scaffolds, which allows for self-aggregation of three-dimensional structures. As a positive control for cytotoxicity, C2C12 cells were grown in a two-dimensional adherent monolayer for the same amount of time. Prior to administering the cytotoxicity reagent, this control was treated with 0.1% TritonX-100 to permeabilize the plasma membrane and release cellular proteases measured by this detection kit. To ensure that the agarose substratum did not interfere with both PrestoBlue cell viability reagent and the CytoTox-Fluor cytotoxicity assay, elastomers and all supernatant containing cells and/or cellular aggregates were transferred to a new 24-well prior to carrying out these assays. Respective reagents were then added to the medium, and the dishes were incubated at 37 °C for 2 h. After this time, both the cell viability via the PrestoBlue cell viability reagent and cytotoxicity via the CytoTox-Fluor cytotoxicity assay were assessed by fluorescence using the multimode microplate reader at 560 nm_{Ex}/590 nm_{Em} and 485 nm_{Ex}/520 nm_{Em}, respectively. All experiments were conducted in biological triplicates.

RESULTS AND DISCUSSION

Synthesis. As starting material, we chose a known nematic (N) main chain LCE constructed from a phenylbenzoate-based reactive monomer as well as cross-linker featuring photopolymerizable acrylate end-groups[64,65] as a representative example for commonly used LCEs. Monomer (M), cross-linker (CL), and photoinitiator (PI) are commercially available. The LCEs were prepared following an oil-in-water (toluene-in-H_2O) microemulsion using hexadecyltrimethylammonium bro-

DOI: 10.1021/acsami.5b04208
ACS Appl. Mater. Interfaces 2015, 7, 14528−14535

mide (CTAB) as surfactant,[66] but otherwise following the common UV-photopolymerization procedure with a standard PI as well as weight fraction between the reactants. These hydrophobic precursors are confined within the toluene droplets after vigorous agitation and the photopolymerization reaction arrests the building blocks in the final structure (see Figure 1). Subsequent evaporation of the water−toluene azeotrope and exhaustive washing and rinsing of the LCE to completely remove the surfactant leaves voids between the LCE globules, thereby introducing porosity into the otherwise dense elastomer. To tune both the morphology and the porosity of the LCEs, we tested adjusting the toluene/H_2O ratio in the microemulsion. Four toluene/H_2O ratios were tested (100/0, 80/20, 50/50, and 20/80) to form the solution (pure toluene) or emulsions that yielded four different LCE samples, which we will refer to as E0, E20, E50 and E80, respectively (Figure 1).

LCE Scaffold Characterization. Morphological studies using scanning electron microscopy (SEM) imaging revealed the globular, porous microstructure of the LCEs featuring spherical microparticles fused together with pores between them. SEM images shown in Figure 2 highlight the morphological changes and progression of changes in the LCEs during the microemulsion synthesis depending on the toluene-H_2O ratio.

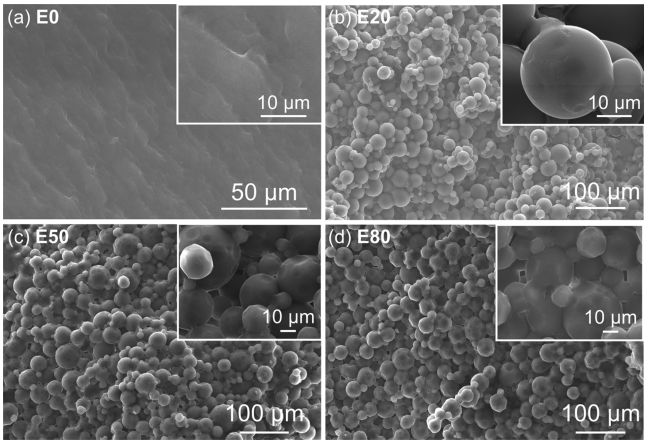

Figure 2. SEM images of LCEs E0−E80 after freeze fracture: (a) E0, (b) E20, (c) E50, and (d) E80. The size distribution of the fused LCE spheres in (b)−(d) ranges from 10 to approximately 30 μm with little variation from 80/20 to 20/80 ratio toluene/H_2O. The LCE quasi-spheres, however, increasingly deviate from an ideal sphere upon increasing the ratio in favor of H_2O (i.e., they display more pronounced faceting).

The SEM micrograph of the freeze-fractured surface of LCE E0 (only toluene) shows a continuous surface, where a slight surface roughness arises from the polydomain nature of the LCE, as observed by other researchers[67] (Figure 2a). The high magnification inset of the same surface shows the dense, nonporous nature of the LCE matrix. Isolated, rarely appearing cavities are likely due to air pockets or microcavities created during the fracturing process. Interestingly, the morphology of the elastomer E20 (toluene/water = 80/20) is quite different from that of E0. The surface is rough, comprised of spherical elastomer particles, fused in an almost closed packed manner (Figure 2b). The structure shows porosity due to the voids formed between the spheres. A closer observation reveals that the LCE particles are about 10−25 μm in diameter with slightly faceted surfaces (inset, Figure 2b). The absence of any contrast within the individual spheres suggests they are compositionally homogeneous. These basic morphological and size features remain the same for E50 (Figure 2c), but the elastomer surface in this case is more faceted and the spherical LCE particles are less densely packed. Visually, the porosity of E50 is only slightly higher than the one of E20. Finally, the appearance of E80 is the most striking, where individual LCE spheres display significant faceting (strongly deviating from ideal spheres) creating what appears to be the most porous among the three LCEs (Figure 2d). Individual faceted spheres have very smooth surfaces and again range in size from 10 to about 30 μm (inset, Figure 2d). Overall, however, the porosity of all three microsphere-based scaffolds (E20, E50, and E80) is quite similar. Both emulsion and microemulsion polymerization have been explored earlier for non-LC polymers and elastomers, and are known to produce similar spherical or globular morphologies.[9,55,59]

All LCE samples were fully characterized using thermal and spectroscopic techniques. The thermal behavior was examined using polarized light optical microscopy (POM) (Figures 3),

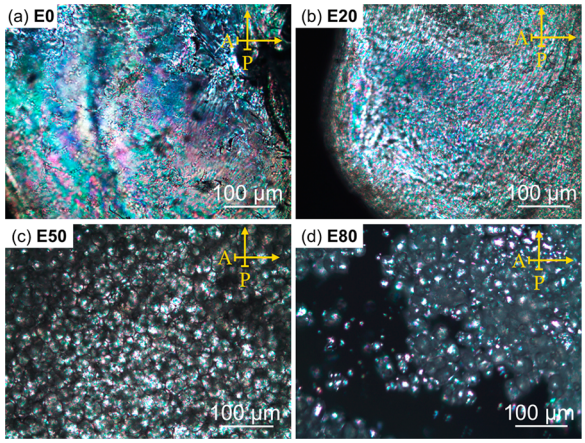

Figure 3. POM micrographs (crossed polarizers) of the nematic LCEs: (a) E0, (b) E20, (c) E50, and (d) E80 of the nematic phase at room temperature.

thermogravimetric analysis (TGA), and differential scanning calorimetry (DSC) (Figures S1 and S2, see the Supporting Information), and the data provide no evidence of any significant difference between the LCEs samples synthesized in pure toluene (E0) or via microemulsion photopolymerization (E20, E50, and E80). The elastomer samples are thermally stable up to at least 200 °C (TGA data) and displayed the following phase sequence (transition temperatures and [enthalpies]): g 7 N 111 [1.0] Iso (°C; [J g^{1-}]) on heating, and Iso 107.5 [0.74] N (°C; [J g^{1-}]) on cooling, as determined by DSC (2nd heating run) and POM. The POM images (Figure 3) support the formation of the nematic phase in all samples, and support the increasing porosity from E20 to E80, based on the area density of the birefringent quasi-spherical domains between crossed polarizers.

Analysis of the all LCE samples by FT-IR spectroscopy revealed no difference between the four LCE samples (Figure S3, see the Supporting Information). This supports that the microemulsion photopolymerization approach does not alter the chemical and thermal properties of the LCEs, but provides a simple means to tailor the morphology that should in

DOI: 10.1021/acsami.5b04208
ACS Appl. Mater. Interfaces 2015, 7, 14528−14535

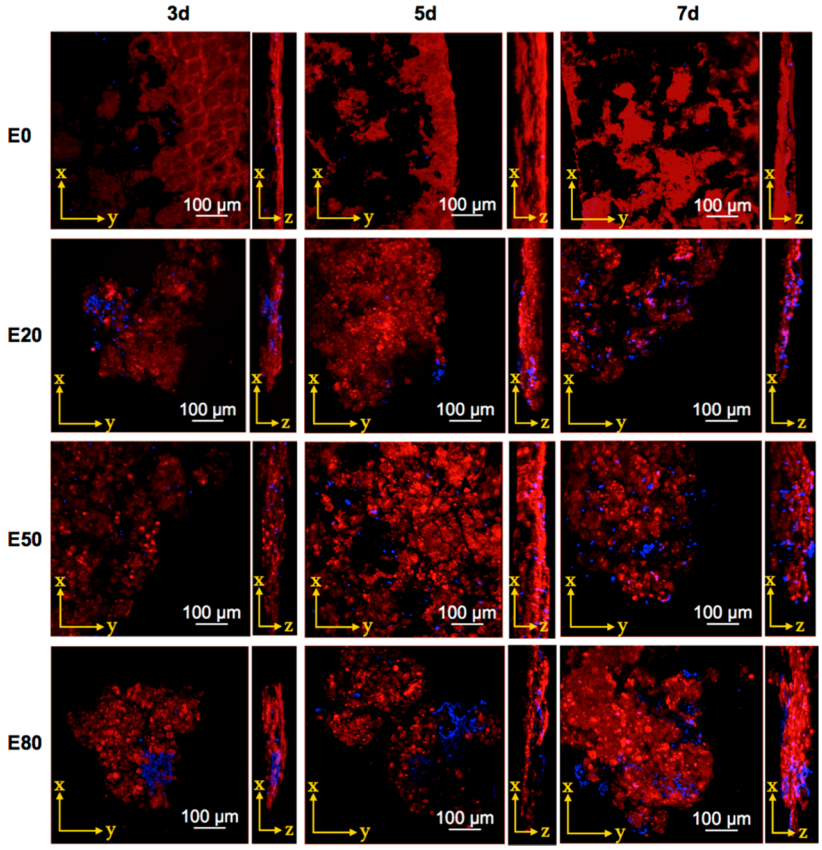

Figure 4. Confocal microscopy images (*x*, *y*-, and *x*,*z*-plane) of C2C12 myoblasts 3, 5, and 7 days after seeding, costained with DAPI for cell nuclei and with rhodamine for the LCE scaffold.

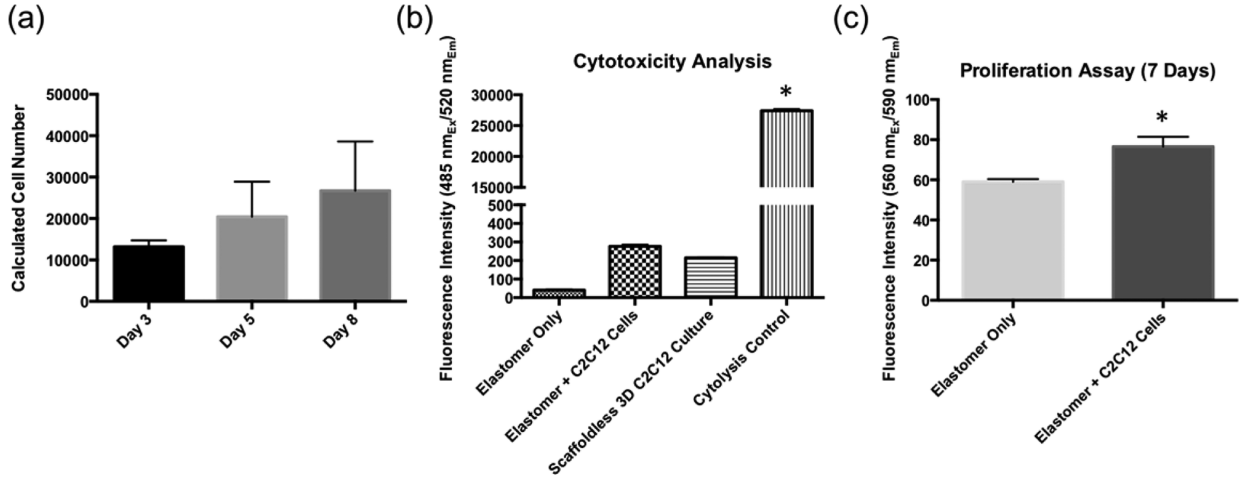

Figure 5. (a) Cell proliferation assay, (b) cytotoxicity assay, and (c) cell viability (*statistically significant change).

principle be suitable for biological application as dynamic and responsive cell scaffolds.

Cell Cultures. To test this hypothesis, all four LCE morphologies with varying levels of smoothness, porosity, and degree of faceting were then tested as cell scaffolds and seeded with muscle cells. C2C12 myoblast cells were cultured and seeded on the surface of the LCEs, which were briefly soaked in poly-D-lysine. The poly-D-lysine treatment is a commonly used technique to promote cell adherence to culture surfaces through a temporary masking of hydrophobic surface properties of the LCEs thus providing an initial, homogeneous net positive charge that is preferred by certain cell types such as C2C12 myoblasts.[68]

After 3 days, cells were found to have adhered directly to the globular LCE surfaces. Cells continued to grow and proliferate within the elastomer matrix. Figure 4 shows the 3D confocal microscopy images of the DAPI (4′,6-diamidino-2-phenylindole) stained nuclei of the C2C12 cells attached to the LCE scaffolds (E0−E80) 3, 5, and 7 days after seeding, respectively, with the LCEs costained with rhodamine. The cells can be seen proliferating only on and within the three globular morphology elastomer morphologies E20, E50, and E80 (the number of cells visually increases with time for all three globular

DOI: 10.1021/acsami.5b04208
ACS Appl. Mater. Interfaces 2015, 7, 14528−14535

morphologies), while the smooth, nonporous E0 elastomer sample does not support the growth and attachment of C2C12 myoblasts as seen in the top row of images in Figure 4.

The surface roughness and the porosity allow the cells to attach better and permeate into the elastomer matrix, therefore showing higher number of cell nuclei. Perhaps the best performing 3D scaffold is the compromise between higher porosity and smoothness of the globular building blocks as well as overall mechanical integrity of the bulk elastomer construct, that is, E50, where the myoblasts can be seen completely permeating into and covering the elastomer's 3D morphology.

Cell Viability, Proliferation, and Cytotoxicity Assays. First, the CyQuant cell proliferation assay was used to provide an accurate and simple measure of the cell number based on the amount of DNA in each cell, which remains constant for a given cell line or cell type. We assessed three time points after seeding the cells (3, 5, and 8 days) for a representative sample of the porous LCE scaffolds (E80). Within the first 3 days of culture, the number of C2C12 cells within the elastomers increased from 10 000 to ∼13 000 cells (±1534). By days 5 and 8, the number of cells had increased further to approximately 20 000 and 26 700 cells (±8454 and 11 875), respectively. The large standard deviations here arise from differences between elastomer pieces, with one showing lower and another one higher cell counts throughout. All, however, showed a steady, essentially linear increase in the total cell number validating cell proliferation on the LCE scaffolds (see Figure 5a and Figure S5 for the standard curve). Thus, the CyQuant cell proliferation assay quantitatively corroborates what was qualitatively observed by confocal microscopy data (Figures 4).

To determine any potential cytotoxic effect of the elastomer scaffolds on C2C12 skeletal myoblasts we employed commercially available cell viability (PrestoBlue cell viability assay) and cytotoxicity assays (CytoTox-Fluor cytotoxicity assay, see Materials and Methods). Biocompatibility data for a structurally related LCE using L929 fibroblast cells, reported by Yakacki et al.[69] as well as data from our earlier work,[52] boded well for the cyto-compatibility of the current LCE materials. The PrestoBlue assay permits the rapid and quantitative evaluation of both cell viability and proliferation. The CytoTox-Fluor assay correlates with the number of dead cells (measuring a distinct protease activity associated with cytotoxicity), analogously to an MTT assay (a colorimetric assay requiring live, active mitochondria using 3-(4,5-dimethylthiazol-2-yl)-2,5-diphenyl tetrazolium bromide) that correlates to the number of live cells. Combining the data from both assays, CytoTox-Fluor and PrestoBlue, for the C2C12 cells seeded onto the LCE scaffolds, together with data for positive and negative control, would allow us to determine whether the LCE scaffolds are biocompatible to muscle cells.

To control for cytotoxicity of the LCEs, we employed both an acellular elastomer culture, as well as a nonadherent cell culture without a scaffold. As a positive control for cytotoxicity, a two-dimensional adherent culture of C2C12 myoblasts were treated with 0.1% TritonX-100 for 30 min prior to conducting the assay. We observed no significant difference in fluorescence intensity in response to the CytoTox-Fluor cytotoxicity assay between acellular scaffolds (scaffold without cells), cellular scaffolds, or scaffold-less self-aggregated cultures. Our positive control for cytotoxicity (TritonX-100 treatment) demonstrated a large, and statistically significant, increase in fluorescence intensity compared to all other groups (Figure 5b).

As a negative control for viability, an acellular elastomer was used. In support of cell viability, after 7 days of culture in growth medium, we detected a significant increase in fluorescence intensity resulting from the PrestoBlue cell viability reagent on cellular versus acellular scaffolds (Figure 5c). Combined, these data demonstrate that the LCE scaffolds employed in this study promote cellular proliferation without any inherent cytotoxicity.

The extent and nature of cell adherence and proliferation clearly depends on the 3D morphology of the LCEs, with the more open structures promoting better cell attachment and growth, particularly within the pores of the microsphere-based scaffolds. Ongoing, long-term studies in our laboratories now focus on the stimuli response of the cell-seeded LCEs and their ability to trigger differentiation, perhaps also alignment, of the C2C12 myoblasts to form myotubes even in the absence of differentiation media (marking the beginning of muscle fiber formation). Considering the unique elastic properties and response of LCEs and the fact that myotubes have been reported to differentiate optimally on substrates with tissue-like stiffness, the proof-of-concept data reported here for the nematic LCEs are especially promising.[70]

CONCLUSIONS

We have demonstrated that nematic LCEs with a globular morphology and intrinsic porosity permit attachment, growth, and proliferation of skeletal muscle cells (C2C12 myoblasts). This is the first study of this kind on the successful use of nematic LCEs that mimic artificial muscle as scaffolds for muscle cells and tissue. In addition, the structural and optical anisotropy of LCEs will be uniquely used in future studies to monitor any changes within the cell construct using techniques such as light scattering or polarized optical microscopy that are not offered by other polymeric cell scaffold materials. With the morphology tailored to function as a scaffold for muscle cells, one can start realizing the various biological uses of LCEs envisioned by de Gennes, Keller, and others. We trust that this study will pave the way for numerous additional biological or medical applications of LCEs, perhaps leading to new research avenues including soft, active medical microdevices as well as implantable biosensors and actuators based on LCEs.

ASSOCIATED CONTENT

Supporting Information

DSC, TGA, and FT-IR data, additional SEM images, and standard plot for cell proliferation assay. The Supporting Information is available free of charge on the ACS Publications website at DOI: 10.1021/acsami.5b04208.

AUTHOR INFORMATION

Corresponding Authors

*E-mail: cmalcuit@kent.edu.
*E-mail: ehegmann@kent.edu.

Author Contributions

The manuscript was written through contributions of all authors. All authors have given approval to the final version of the manuscript.

Notes

The authors declare no competing financial interest.

DOI: 10.1021/acsami.5b04208
ACS Appl. Mater. Interfaces 2015, 7, 14528−14535

■ ACKNOWLEDGMENTS

We thank KSU for financial support of the Regenerative Medicine Initiative at Kent State (ReMedIKS). T.H. gratefully acknowledges financial support from the Government of Ohio's Third Frontier Program for Ohio Research Scholars.

■ REFERENCES

(1) Page, R. L.; Malcuit, C.; Vilner, L.; Vojtic, I.; Shaw, S.; Hedblom, E.; Hu, J.; Pins, G. D.; Rolle, M. W.; Dominko, T. Restoration of Skeletal Muscle Defects with Adult Human Cells Delivered on Fibrin Microthreads. *Tissue Eng., Part A* **2011**, *17* (21−22), 2629−2640.

(2) Brand, H. R.; Finkelmann, H. Physcial Properties of Liquid Crystalline Elastomers. In *Handbook of Liquid Crystals*; Demus, D., Goodby, J. W., Gray, G. W., Spiess, H. W., Vill, V., Eds.; Wiley: New York, 2008; Vol. *3*, pp 277−302.

(3) de Jeu, W. H. E. *Liquid Crystal Elastomers: Materials and Applications*; Springer: New York, 2012.

(4) Wei, R. B.; Zhang, H. X.; He, Y. N.; Wang, X. G.; Keller, P. Photoluminescent Nematic Liquid Crystalline Elastomer Actuators. *Liq. Cryst.* **2014**, *41* (12), 1821−1830.

(5) Torras, N.; Zinoviev, K. E.; Camargo, C. J.; Campo, E. M.; Campanella, H.; Esteve, J.; Marshall, J. E.; Terentjev, E. M.; Omastova, M.; Krupa, I.; Teplicky, P.; Mamojka, B.; Bruns, P.; Roeder, B.; Vallribera, M.; Malet, R.; Zuffanelli, S.; Soler, V.; Roig, J.; Walker, N.; Wenn, D.; Vossen, F.; Crompvoets, F. M. H. Tactile Device Based on Opto-Mechanical Actuation of Liquid Crystal Elastomers. *Sens. Actuators, A* **2014**, *208*, 104−112.

(6) Torras, N.; Marshall, J. E.; Zinoviev, K. E.; Camargo, C. J.; Terentjev, E. M.; Esteve, J. Gas-Pressure Molding-Based Fabrication of Smart Actuators from Nematic Liquid-Crystalline Elastomer. *Macromol. Mater. Eng.* **2014**, *299* (10), 1163−1169.

(7) Schenning, A. P. H. J.; Bastiaansen, C. M. W.; Broer, D. J.; Debije, M. G. The Role of Supramolecular Chemistry in Stimuli Responsive and Hierarchically Structured Functional Organic Materials. *Chim. Oggi* **2014**, *32* (3), 78−80.

(8) Pei, Z. Q.; Yang, Y.; Chen, Q. M.; Terentjev, E. M.; Wei, Y.; Ji, Y. Mouldable Liquid-Crystalline Elastomer Actuators with Exchangeable Covalent Bonds. *Nat. Mater.* **2014**, *13* (1), 36−41.

(9) Marshall, J. E.; Gallagher, S.; Terentjev, E. M.; Smoukov, S. K. Anisotropic Colloidal Micromuscles from Liquid Crystal Elastomers. *J. Am. Chem. Soc.* **2014**, *136* (1), 474−479.

(10) Kim, C.; Mukherjee, S.; Luchette, P.; Palffy-Muhoray, P. Director Orientation in Deformed Liquid Crystal Elastomer Microparticles. *Soft Mater.* **2014**, *12* (2), 159−165.

(11) Ohm, C.; Brehmer, M.; Zentel, R. Applications of Liquid Crystalline Elastomers. In *Liquid Crystal Elastomers: Materials and Applications*; de Jeu, W. H., Ed.; Springer: New York, 2012; Vol. *250*, pp 49−93.

(12) Ji, Y.; Marshall, J. E.; Terentjev, E. M. Nanoparticle-Liquid Crystalline Elastomer Composites. *Polymers (Basel, Switz.)* **2012**, *4* (1), 316−340.

(13) Fleischmann, E. K.; Liang, H. L.; Kapernaum, N.; Giesselmann, F.; Lagerwall, J.; Zentel, R. One-Piece Micropumps from Liquid Crystalline Core-Shell Particles. *Nat. Commun.* **2012**, *3*, 1178.

(14) Broer, D. J.; Bastiaansen, C. M. W.; Debije, M. G.; Schenning, A. P. H. J. Functional Organic Materials Based on Polymerized Liquid-Crystal Monomers: Supramolecular Hydrogen-Bonded Systems. *Angew. Chem., Int. Ed.* **2012**, *51* (29), 7102−7109.

(15) Sanchez-Ferrer, A.; Fischl, T.; Stubenrauch, M.; Albrecht, A.; Wurmus, H.; Hoffmann, M.; Finkelmann, H. Liquid-Crystalline Elastomer Microvalve for Microfluidics. *Adv. Mater.* **2011**, *23* (39), 4526−4530.

(16) Ahn, S. K.; Deshmukh, P.; Gopinadhan, M.; Osuji, C. O.; Kasi, R. M. Side-Chain Liquid Crystalline Polymer Networks: Exploiting Nanoscale Smectic Polymorphism to Design Shape-Memory Polymers. *ACS Nano* **2011**, *5* (4), 3085−3095.

(17) Ohm, C.; Brehmer, M.; Zentel, R. Liquid Crystalline Elastomers as Actuators and Sensors. *Adv. Mater.* **2010**, *22* (31), 3366−3387.

(18) van Oosten, C. L.; Bastiaansen, C. W. M.; Broer, D. J. Printed Artificial Cilia from Liquid-Crystal Network Actuators Modularly Driven by Light. *Nat. Mater.* **2009**, *8* (8), 677−682.

(19) Vennes, M.; Martin, S.; Gisler, T.; Zentel, R. Anisotropic Particles from LC Polymers for Optical Manipulation. *Macromolecules* **2006**, *39* (24), 8326−8333.

(20) Ahir, S. V.; Tajbakhsh, A. R.; Terentjev, E. M. Self-Assembled Shape-Memory Fibers of Triblock Liquid-Crystal Polymers. *Adv. Funct. Mater.* **2006**, *16* (4), 556−560.

(21) Ahir, S. V.; Terentjev, E. M. Photomechanical Actuation in Polymer-Nanotube Composites. *Nat. Mater.* **2005**, *4* (6), 491−495.

(22) Lehmann, W.; Skupin, H.; Tolksdorf, C.; Gebhard, E.; Zentel, R.; Kruger, P.; Losche, M.; Kremer, F. Giant Lateral Electrostriction in Ferroelectric Liquid-Crystalline Elastomers. *Nature* **2001**, *410* (6827), 447−450.

(23) Palffy-Muhoray, P.; Meyer, R. B. Bridging the Experiment-Theory Gap. *Nat. Mater.* **2004**, *3* (3), 139−140.

(24) Camacho-Lopez, M.; Finkelmann, H.; Palffy-Muhoray, P.; Shelley, M. Fast Liquid-Crystal Elastomer Swims into the Dark. *Nat. Mater.* **2004**, *3* (5), 307−310.

(25) Sanchez-Ferrer, A.; Finkelmann, H. Opto-Mechanical Effect in Photoactive Nematic Main-Chain Liquid-Crystalline Elastomers. *Soft Matter* **2013**, *9* (18), 4621−4627.

(26) Brommel, F.; Kramer, D.; Finkelmann, H. Preparation of Liquid Crystalline Elastomers. In *Liquid Crystal Elastomers: Materials and Applications*; de Jeu, W. H., Ed.; Springer: New York, 2012; Vol. *250*, pp 1−48.

(27) Zander, F.; Finkelmann, H. State of Order of the Crosslinker in Main-Chain Liquid Crystalline Elastomers. *Macromol. Chem. Phys.* **2010**, *211* (10), 1167−1176.

(28) Rozic, B.; Krause, S.; Finkelmann, H.; Cordoyiannis, G.; Kutnjak, Z. Controlling the Thermomechanical Response of Liquid-Crystalline Elastomers by Influencing their Critical Behavior. *Appl. Phys. Lett.* **2010**, *96* (11), 111901.

(29) Sanchez-Ferrer, A.; Finkelmann, H. Thermal and Mechanical Properties of New Main-Chain Liquid-Crystalline Elastomers. *Mol. Cryst. Liq. Cryst.* **2009**, *508*, 348−356.

(30) Chambers, M.; Finkelmann, H.; Remskar, M.; Sanchez-Ferrer, A.; Zalar, B.; Žumer, S. Liquid Crystal Elastomer-Nanoparticle Systems for Actuation. *J. Mater. Chem.* **2009**, *19* (11), 1524−1531.

(31) de Jeu, W. H.; Obraztsov, E. P.; Ostrovskii, B. I.; Ren, W.; McMullan, P. J.; Griffin, A. C.; Sanchez-Ferrer, A.; Finkelmann, H. Order and Strain in Main-Chain Smectic Liquid-Crystalline Polymers and Elastomers. *Eur. Phys. J. E* **2007**, *24* (4), 399−409.

(32) Martinoty, P.; Stein, P.; Finkelmann, H.; Pleiner, H.; Brand, H. R. Mechanical Properties of Monodomain Side Chain Nematic Elastomers. *Eur. Phys. J. E* **2004**, *14* (4), 311−321.

(33) Cao, W.; Finkelmann, H.; Kim, S. T.; Munoz, A.; Palffy-Muhoray, P.; Taheri, B.; Twieg, R. Mirrorless Lasing in Liquid Crystalline Materials. *Proc. SPIE* **2002**, *4642*, 55−61.

(34) Stein, P.; Assfalg, N.; Finkelmann, H.; Martinoty, P. Shear Modulus of Polydomain, Mono-Domain and Non-Mesomorphic Side-Chain Elastomers: Influence of the Nematic Order. *Eur. Phys. J. E* **2001**, *4* (3), 255−262.

(35) Lehmann, W.; Hartmann, L.; Kremer, F.; Stein, P.; Finkelmann, H.; Kruth, H.; Diele, S. Direct and Inverse Electromechanical Effect in Ferroelectric Liquid Crystalline Elastomers. *J. Appl. Phys.* **1999**, *86* (3), 1647−1652.

(36) Agrawal, A.; Yun, T. H.; Pesek, S. L.; Chapman, W. G.; Verduzco, R. Shape-Responsive Liquid Crystal Elastomer Bilayers. *Soft Matter* **2014**, *10* (9), 1411−1415.

(37) Agrawal, A.; Chipara, A. C.; Shamoo, Y.; Patra, P. K.; Carey, B. J.; Ajayan, P. M.; Chapman, W. G.; Verduzco, R. Dynamic Self-Stiffening in Liquid Crystal Elastomers. *Nat. Commun.* **2013**, *4*, 1739.

(38) Garcia-Amoros, J.; Martinez, M.; Finkelmann, H.; Velasco, D. Photoactuation and Thermal Isomerisation Mechanism of Cyanoazobenzene-Based Liquid Crystal Elastomers. *Phys. Chem. Chem. Phys.* **2014**, *16* (18), 8448−8454.

DOI: 10.1021/acsami.5b04208
ACS Appl. Mater. Interfaces 2015, 7, 14528−14535

(39) Fleischmann, E. K.; Zentel, R. Liquid-Crystalline Ordering as a Concept in Materials Science: From Semiconductors to Stimuli-Responsive Devices. *Angew. Chem., Int. Ed.* **2013**, *52* (34), 8810−8827.
(40) Li, M. H.; Keller, P. Artificial Muscles Based on Liquid Crystal Elastomers. *Philos. Trans. R. Soc., A* **2006**, *364* (1847), 2763−2777.
(41) Mayer, S.; Zentel, R. Liquid Crystalline Polymers and Elastomers. *Curr. Opin. Solid State Mater. Sci.* **2002**, *6* (6), 545−551.
(42) Finkelmann, H.; Shahinpoor, M. Electrically-Controllable Liquid Crystal Elastomer-Graphite Composite Artificial Muscles. *Proc. SPIE* **2002**, *4695*, 459−464.
(43) Buguin, A.; Li, M. H.; Silberzan, P.; Ladoux, B.; Keller, P. Micro-actuators: When Artificial Muscles Made of Nematic Liquid Crystal Elastomers Meet Soft Lithography. *J. Am. Chem. Soc.* **2006**, *128* (4), 1088−1089.
(44) Shenoy, D. K.; Thomsen, D. L.; Srinivasan, A.; Keller, P.; Ratna, B. R. Carbon Coated Liquid Crystal Elastomer Film for Artificial Muscle Applications. *Sens. Actuators, A* **2002**, *96* (2−3), 184−188.
(45) Thomsen, D. L.; Keller, P.; Naciri, J.; Pink, R.; Jeon, H.; Shenoy, D.; Ratna, B. R. Liquid Crystal Elastomers with Mechanical Properties of a Muscle. *Macromolecules* **2001**, *34* (17), 5868−5875.
(46) Ratna, B. R.; Thomsen, D. L.; Keller, P. Liquid Crystal Elastomers as Artificial Muscles: Role of Side-Chain-Backbone Coupling. *Proc. SPIE* **2001**, *4329*, 233−237.
(47) De Gennes, P. G.; Hébert, M.; Kant, R. Artificial Muscles Based on Nematic Gels. *Macromol. Symp.* **1997**, *113*, 39−49.
(48) de Gennes, P.-G. A Semi-Fast Artificial Muscle. *C. R. Acad. Sci. Paris, Ser. IIb* **1997**, *324*, 343−348.
(49) Mitragotri, S.; Lahann, J. Physical Approaches to Biomaterial Design. *Nat. Mater.* **2009**, *8* (1), 15−23.
(50) Kodali, A.; Lim, T. C.; Leong, D. T.; Tong, Y. W. Cell-Microsphere Constructs Formed with Human Adipose-Derived Stem Cells and Gelatin Microspheres Promotes Stemness, Differentiation, and Controlled Pro-Angiogenic Potential. *Macromol. Biosci.* **2014**, *14* (10), 1458−1468.
(51) Discher, D. E.; Janmey, P.; Wang, Y. L. Tissue Cells Feel and Respond to the Stiffness of their Substrate. *Science* **2005**, *310* (5751), 1139−1143.
(52) Sharma, A.; Neshat, A.; Mahnen, C. J.; Nielsen, A. d.; Snyder, J.; Stankovich, T. L.; Daum, B. G.; LaSpina, E. M.; Beltrano, G.; Li, S.; Park, B.-W.; Clements, R. J.; Freeman, E. J.; Malcuit, C.; McDonough, J. A.; Korley, L. T. J.; Hegmann, T.; Hegmann, E. Biocompatible, Biodegradable and Porous Liquid Crystal Elastomer Scaffolds for Spatial Cell Cultures. *Macromol. Biosci.* **2015**, *15*, 200−214.
(53) Haseloh, S.; Ohm, C.; Smallwood, F.; Zentel, R. Nanosized Shape-Changing Colloids from Liquid Crystalline Elastomers. *Macromol. Rapid Commun.* **2011**, *32* (1), 88−93.
(54) Haseloh, S.; van der Schoot, P.; Zentel, R. Control of Mesogen Configuration in Colloids of Liquid Crystalline Polymers. *Soft Matter* **2010**, *6* (17), 4112−4119.
(55) Spillmann, C. M.; Naciri, J.; Wahl, K. J.; Garner, Y. H.; Chen, M. S.; Ratna, B. R. Role of Surfactant in the Stability of Liquid Crystal-Based Nanocolloids. *Langmuir* **2009**, *25* (4), 2419−2426.
(56) Haseloh, S.; Zentel, R. Synthesis of Liquid-Crystalline Colloids in Nonpolar Media and their Manipulation in Electric Fields. *Macromol. Chem. Phys.* **2009**, *210* (17), 1394−1401.
(57) Lange, B.; Metz, N.; Tahir, M. N.; Fleischhaker, F.; Theato, P.; Schroder, H. C.; Muller, W. E. G.; Tremel, W.; Zentel, R. Functional Polymer-Opals from Core-Shell Colloids. *Macromol. Rapid Commun.* **2007**, *28* (20), 1987−1994.
(58) Yang, Z. Q.; Huck, W. T. S.; Clarke, S. M.; Tajbakhsh, A. R.; Terentjev, E. M. Shape-Memory Nanoparticles from Inherently Non-Spherical Polymer Colloids. *Nat. Mater.* **2005**, *4* (6), 486−490.
(59) Vennes, M.; Zentel, R.; Rossle, M.; Stepputat, M.; Kolb, U. Smectic Liquid-Crystalline Colloids by Miniemulsion Techniques. *Adv. Mater.* **2005**, *17* (17), 2123−2127.
(60) Missirlis, D.; Tirelli, N.; Hubbell, J. A. Amphiphilic Hydrogel Nanoparticles. Preparation, Characterization, and Preliminary Assessment as New Colloidal Drug Carriers. *Langmuir* **2005**, *21* (6), 2605−2613.
(61) Vennes, M.; Zentel, R. Liquid-Crystalline Colloidal Particles. *Macromol. Chem. Phys.* **2004**, *205* (17), 2303−2311.
(62) Egen, M.; Zentel, R. Surfactant-Free Emulsion Polymerization of Various Methacrylates: Towards Monodisperse Colloids for Polymer Opals. *Macromol. Chem. Phys.* **2004**, *205* (11), 1479−1488.
(63) Rasband, W. S. *ImageJ*; U.S. National Institutes of Health: Bethesda, MD, 1997−2015; http://imagej.nih.gov/ij/.
(64) Lub, J.; Broer, D. J.; Wegh, R. T.; Peeters, E.; van der Zande, B. M. I. Formation of Optical Films by Photo-Polymerisation of Liquid Crystalline Acrylates and Application of these Films in Liquid Crystal Display Technology. *Mol. Cryst. Liq. Cryst.* **2005**, *429*, 77−99.
(65) Harris, K. D.; Cuypers, R.; Scheibe, P.; van Oosten, C. L.; Bastiaansen, C. W. M.; Lub, J.; Broer, D. J. Large Amplitude Light-Induced Motion in High Elastic Modulus Polymer Actuators. *J. Mater. Chem.* **2005**, *15* (47), 5043−5048.
(66) Peinado, C.; Bosch, P.; Martin, V.; Corrales, T. Photoinitiated Polymerization in Bicontinuous Microemulsions: Fluorescence Monitoring. *J. Polym. Sci., Polym. Chem.* **2006**, *44* (18), 5291−5303.
(67) Higaki, H.; Urayama, K.; Takigawa, T. Memory and Development of Textures of Polydomain Nematic Elastomers. *Macromol. Chem. Phys.* **2012**, *213* (18), 1907−1912.
(68) Ciofani, G.; Ricotti, L.; Danti, S.; Moscato, S.; Nesti, C.; D'Alessandro, D.; Dinucci, D.; Chiellini, F.; Pietrabissa, A.; Petrini, M.; Menciassi, A. Investigation of Interactions between Poly-L-Lysine-Coated Boron Nitride Nanotubes and C2C12 Cells: Up-Take, Cytocompatibility, and Differentiation. *Int. J. Nanomed.* **2010**, *5*, 285−298.
(69) Yakacki, C. M.; Saed, M.; Nair, D. P.; Gong, T.; Reed, S. M.; Bowman, C. N. Tailorable and Programmable Liquid-Crystalline Elastomers using a Two-Stage Thiol−Acrylate Reaction. *RSC Adv.* **2015**, *5*, 18997−19001.
(70) Engler, A. J.; Griffin, M. A.; Sen, S.; Bonnetnann, C. G.; Sweeney, H. L.; Discher, D. E. Myotubes Differentiate Optimally on Substrates with Tissue-Like Stiffness: Pathological Implications for Soft or Stiff Microenvironments. *J. Cell Biol.* **2004**, *166* (6), 877−887.

DOI: 10.1021/acsami.5b04208
ACS Appl. Mater. Interfaces 2015, 7, 14528−14535